Short communication

Nano-structured spherical porous SnO$_2$ anodes for lithium-ion batteries

L. Yuan [*], Z.P. Guo, K. Konstantinov, H.K. Liu, S.X. Dou

Institute of Superconducting & Electronic Materials, University of Wollongong, NSW 2522, Australia

Abstract

Spherical porous tin oxide was fabricated via a spray pyrolysis technique. TEM revealed that the primary SnO$_2$ crystals had an average size of about 5 nm. The electrochemical measurements showed that the spherical porous SnO$_2$ samples have excellent cyclability, which can deliver a reversible capacity of $410 \, \text{mAh g}^{-1}$ up to 50 cycles as a negative electrode for lithium batteries. The second step of the study was to thermal treat the initial tin oxide for 3 h at 600, 800, 1000 and 1200 °C, respectively, in order to identify the particle size effect on the electrochemical performance toward lithium. It was found that the morphologies of these spherical clusters could be maintained even after thermal treatment at 1200 °C. It was also proved that finer the size of the tin oxide particles the better the electrochemical performance.
© 2006 Elsevier B.V. All rights reserved.

Keywords: Lithium-ion; Anodes; SnO$_2$; Tin; Nano-particles

1. Introduction

As a major breakthrough in the hybrid vehicle field, lithium-ion batteries still need to be further improved to meet ongoing market innovations. Much research work is presently directed towards the exploration of different types of materials with high reversible capacity and long cycle life. With respect to the anode, the main goal is to replace the present carbon-based materials with larger specific capacity materials, i.e. metals or compounds that alloy with lithium (e.g. Sn, Si, Sb, etc.) [1,2]. As possible anodes for next generation lithium-ion batteries, tin oxide-based materials show great promise for their high storage capacity [3]. However, as is always observed, the significant capacity fading of these anodes has undermined the advantage. A popular approach to counter particle pulverization is to reduce the particle size of the tin oxide to give a small absolute volume change in the local environment. The amorphous or nanocrystalline electrode in the Li$_2$O matrix may prevent aggregation of tin region [4,5]. The use of nanosized particles in electrodes could not only reduce the diffusion length for lithium insertion but also decrease the charge-transfer resistance of the electrodes. In addition, the higher surface area of nanosized tin oxide particles could lead to higher catalytic efficiency of anodes. Various techniques have been used to prepare nanosized tin oxide, including

conventional precipitation [6], homogeneous precipitation [7], a surfactant-mediated method [8], the sol–gel method, reverse microemulsion [9,10], etc. In this paper, experiments using the spray pyrolysis technique are emphasized because it is a suitable method for mass production. While other preparation methods give rather randomly aggregated particles with larger grain sizes, the spray pyrolysis method produces hollow spheres typically 0.5–1 μm in diameter composed of crystals of about 5 nm. The detailed microscopic features and the electrochemical performance of the spherical porous tin oxide materials were both studied.

2. Experimental

One molar SnCl$_2$ ethanol solution was prepared as the precursor solution. The solution was then fed into a vertical spray pyrolysis reactor. An atomizing nozzle was used in combination with compressed air. The liquid was fed at a rate of $100 \, \text{ml min}^{-1}$, and the spraying was carried out at a pressure of 2.0 MPa and an atmospheric temperature of 700 °C to produce tin oxides. Then the initial as prepared tin oxides were thermal treated in air for 3 h at 600, 800, 1000 and 1200 °C, respectively. Powder X-ray diffraction (1730 Philips X-ray diffractometer) using Cu Kα radiation was employed to identify the crystalline phase of the synthesized materials. The morphology of the resulting oxides was observed using a scanning electron microscope (SEM) (Leica Cambridge Steroscan 440). Transmission electron microscope (TEM) images and high resolution (HR) TEM

---

[*] Corresponding author. Tel.: +61 2 4221 3017; fax: +61 2 4221 5731.
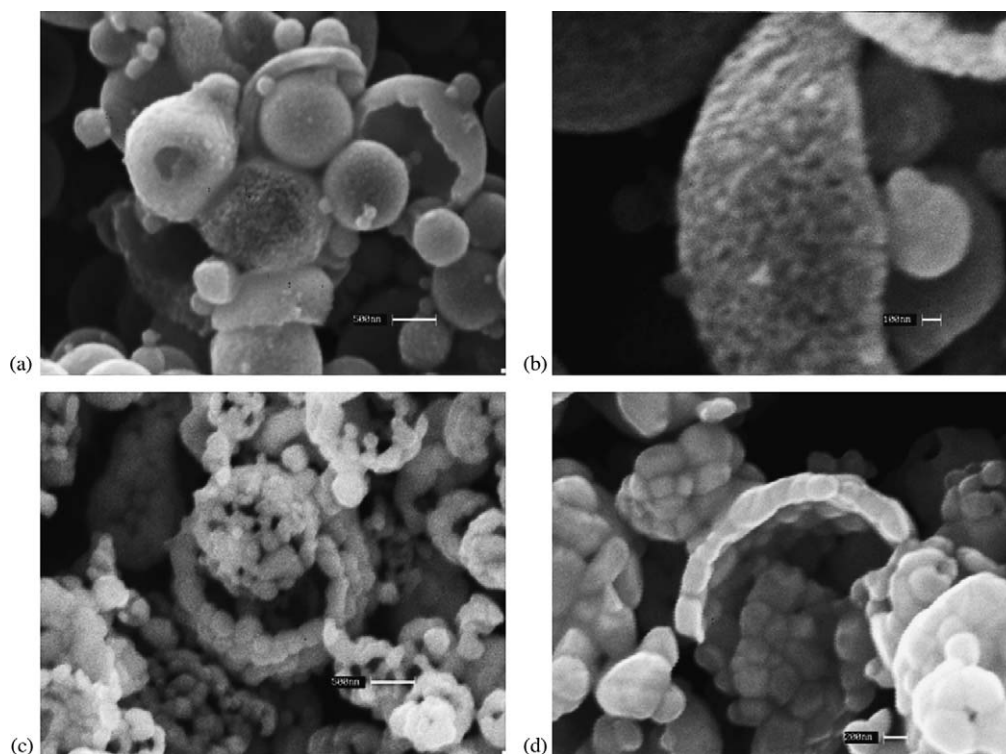*E-mail address:* ly93@uow.edu.au (L. Yuan).

Fig. 1. SEM images of (a) initial sprayed SnO_2 and SnO_2 samples followed by thermal treatment in air at (b) 800 °C, (c) 1000 °C and (d) 1200 °C.

were obtained from a Philips M12 and JEOL F3000 microscope. Anodes were made for electrochemical testing, by dispersing 80% active materials, 15% acetylene carbon black and 5% poly (vinylidene fluoride) in a solvent of dimethyl phthalate. The slurry was then coated on copper foils to a mass loading of about 1 mg and then dried at 140 °C and pressed at 150 kg cm^{-2}. CR2032 coin cells were assembled in an argon-filled glove box. The counter electrode was Li metal and the electrolyte was 1 M $LiPF_6$ dissolved in a 50:50 (v/v) mixture of ethylene carbonate (EC) and dimethyl carbonate (DMC) provided by MERCK KgaA, Germany. These cells were cycled between 0.05 and 1.35 V at room temperature.

3. Results and discussion

3.1. Physical and structural characterization

Fig. 1 shows SEM images of the initial as prepared SnO_2 and SnO_2 samples followed by thermal treatment in air at 800, 1000 and 1200 °C. Spherical morphology with a highly porous, foam-like structure can be observed. The diameter of the porous hollow spheres is from 0.5 to 1 μm. It is conceivable that the small pores inside the walls originate mainly from the high-speed spray gas. Fig. 1(c and d) shows that the spheres have aggregated after thermal treatment at higher temperatures. However, the morphologies of these spherical clusters can be maintained even after thermal treatment at 1200 °C. Fig. 2 shows the X-ray powder patterns of the SnO_2 samples. Table 1.displays the specific surface areas and calculated crystal size of the SnO_2 samples.
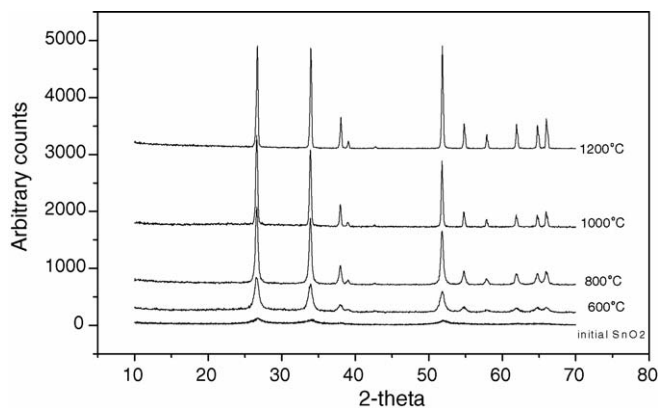

Fig. 2. X-ray powder patterns of initial as prepared SnO_2 and SnO_2 samples followed by thermal treatment in air at 600, 800, 1000 and 1200 °C, respectively.

Table 1
The specific surface areas and calculated crystal size of the SnO_2 sample

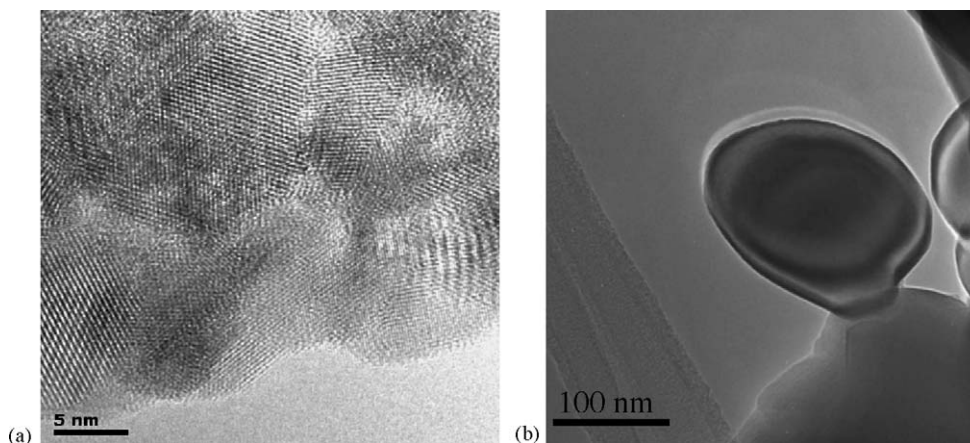| Samples	Specific surface area (m^2 g^{-1})	Calculated SnO_2 crystal size (nm)
Commercial SnO_2 (Aldrich, 99%)	7.2	–
Initial SnO_2	28.4	5.1
600 °C SnO_2	20.5	12.92
800 °C SnO_2	17.0	32.97
1000 °C SnO_2	11.5	53.86
1200 °C SnO_2	6.6	101.01

Fig. 3. HRTEM images of (a) the initial as prepared SnO_2 and (b) the thermal treated SnO_2 (1200 °C).

The crystallite size of SnO_2 was determined from the Bragg peaks using the Scherer formula [11]:

$$d = k\lambda\beta^{-1}\cos\theta^{-1}$$

where $k = 0.89$, λ is the X-ray wavelength, θ the Bragg angle, and β is the real half-peak width in radians after corrections for instrument broadening. As we can see, with the thermal treatment temperature increasing, the SnO_2 crystallites grew larger and larger (from 5.1 to 101 nm) and the specific surface areas decreased from 28.4 to 6.6 $m^2\,g^{-1}$. Close examination of samples by high resolution TEM revealed that the initial SnO_2 crystals have an average size of about 5 nm (Fig. 3(a)). Good interconnection between crystals is also observed. Fig. 3(b) confirmed that SnO_2 crystals have grown to an average size of about 100 nm after 1200 °C thermal treatment.

3.2. Electrochemical characterization

The specific capacity and cycling stability of SnO_2 electrodes were measured by constant current charge/discharge testing. Fig. 4 shows voltage profiles of the spherical porous SnO_2 electrode at the 1st, 2nd, 10th and 20th cycle at a current density of
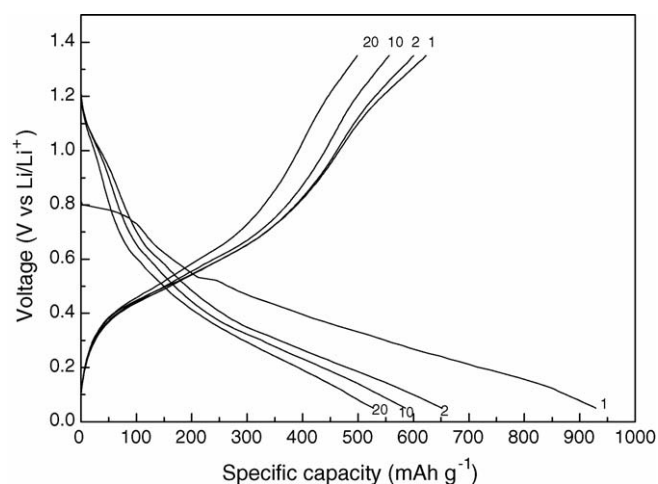

Fig. 4. Voltage profiles of the initial as prepared spherical porous SnO_2 electrode at the 1st, 2nd, 10th and 20th cycle at a current density of 100 mA g^{-1}.

100 mA g^{-1}. The SnO_2 anode shows a large initial irreversible capacity (328 mAh g^{-1}). The CV curves (Fig. 5) for the two electrodes clearly indicate the irreversible reaction during the first discharge with a reduction peak at 0.8–0.9 V. It is also observed
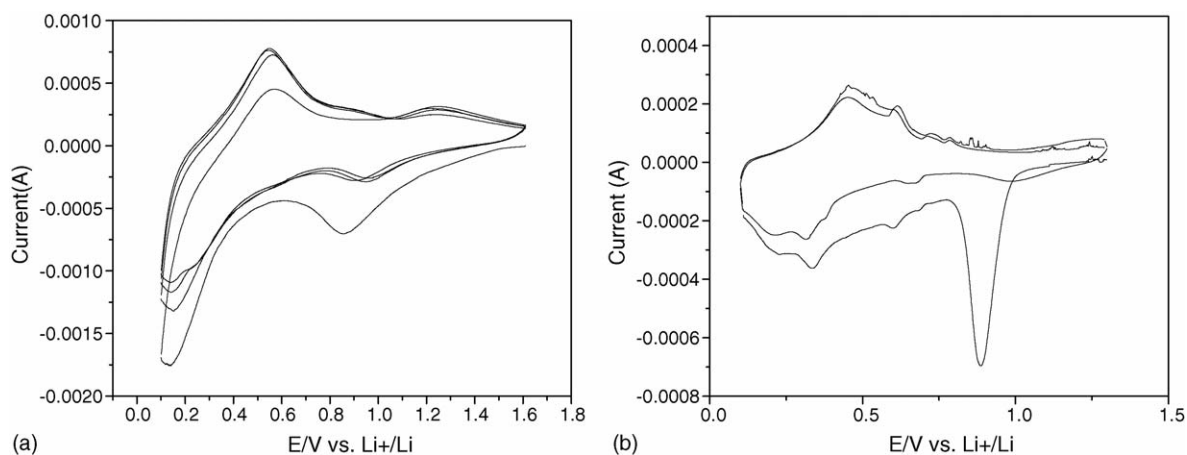

Fig. 5. Cyclic voltammograms for (a) the initial as prepared SnO_2 electrode and (b) the thermal treated SnO_2 electrode (1200 °C). Scan rate 0.1 mV s^{-1}.
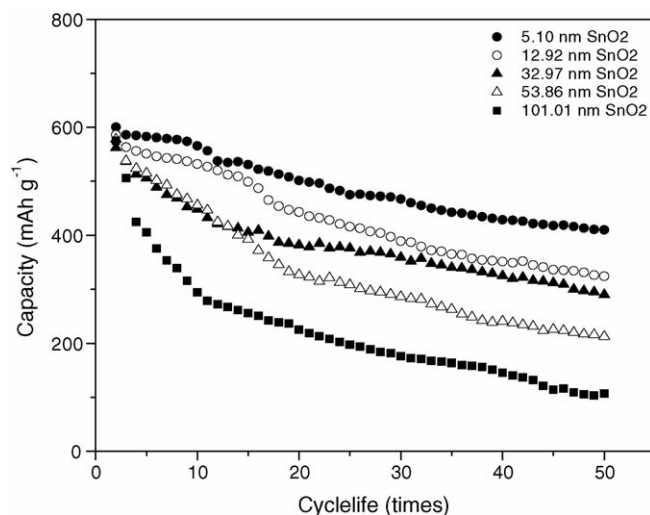
Fig. 6. Discharge capacity vs. cycle number for the potential range from 0.05 to 1.35 V for the initial as prepared SnO_2, and the thermal treated SnO_2 samples with different crystals average size.

that the initial as prepared spherical porous SnO_2 shows a much smoother CV curves. This suggests that the two-phase regions in the tin particles have been suppressed in the sample, thereby preventing grain cracking and fragmentation, and the cycle stability of the SnO_2 electrode is therefore better. Fig. 6 compares the discharge capacity versus the number of charge/discharge cycles for the SnO_2 samples. The initial as prepared spherical porous SnO_2 (5.1 nm) exhibits excellent cycle stability: the retentive capacity (410 mAh g^{-1}) up to 50 cycles is 68.2% of the initial capacity (601 mAh g^{-1}). The 12.92, 32.97, 53.86 and 101.01 nm SnO_2 electrodes remained at 54.6, 51.6, 36.7 and 18.5%, respectively, of their initial discharging capacity. It shows how much a change in the particle size of the anode can strongly affect the capacity retention. It was proved that the finer the size of the tin oxide particles the better the electrochemical cycle stability.

4. Conclusions

Spherical porous tin oxide fabricated via a spray pyrolysis technique showed excellent cycle stability. We believe that the spherical clusters of SnO_2 nanocrystals form a flexible, three-dimensional porous framework such that the porous structure does not collapse during charge and discharge. The pores between nanosized particles reduce the possibility of tin aggregation, and in the meanwhile, they act as a "buffer zone" which accommodates the volume change of the tin phase during Li alloying/de-alloying. The spherical porous structure plays a significant role in retaining the capacity. Moreover, the particle size effect on the electrochemical performance toward lithium has been identified. We show that a decrease in particle size improves the material cycling stability.

References

[1] J.L. Tirado, Mater. Sci. Eng. R40 (2003) 103–136.
[2] Y. Idota, US Patent, 5,478,671 (1995).
[3] Y. Idota, A. Matsufuji, Y. Mackawa, T. Miyasaka, Science 276 (1997) 1395.
[4] P. Poizot, S. Laruelle, S. Grugeon, L. Dupont, J.-M. Tarascon, Nature 407 (2000) 496.
[5] N. Zheng, X. Bu, P. Feng, Nature 426 (2003) 428.
[6] G.J. Li, S. Kawi, Mater. Lett. 34 (1998) 99.
[7] K.C. Song, Y. Kang, Mater. Lett. 42 (2000) 283.
[8] Y. Wang, C. Ma, X. Sun, H. Li, Nanotechnology 13 (2002) 565.
[9] H. Li, X. Huang, L. Chen, J. Power Sources 81–82 (1999) 335.
[10] A. Jitianu, Y. Altindag, M. Zaharescu, M. Wark, J. Sol–Gel Sci. Technol. 26 (2003) 483.
[11] C.S. Wang, G.T. Wu, X.B. Zhang, Z.F. Qi, W.Z. Li, J. Electrochem. Soc. 145 (1998) 2751.